Multi-intermediate-band character of Ti-substituted $CuGaS_2$: Implications for photovoltaic applications

J. Hashemi, A. Akbari, S. Huotari, and M. Hakala
Department of Physics, University of Helsinki, P.O. Box 64, FI-00014, Helsinki, Finland
(Received 28 April 2014; revised manuscript received 24 July 2014; published 29 August 2014)

Intermediate-band (IB) photovoltaic materials are designed to absorb a wider range of the solar spectrum by dividing the gap with a set of bands that plays a mediating role in two-step absorption processes. Thus far, the conventional model of IB absorbers has been focused on a single half-filled IB. We show that a multiple-IB picture with filled and empty bands provides a more convincing explanation of the experimental findings in some cases, and it should be considered as a possible scenario in understanding and engineering IB solar cells. Toward that end, we report the formation of two sets of IBs in a Ti-substituted $CuGaS_2$ compound. Using hybrid functional calculations within the density functional theory framework, we show that the lower IBs are occupied and mainly derive from the Ti $3d_{x^2-y^2}$ states, while the higher ones originate from the Ti $3d_{z^2}$ states and are unoccupied. The positions of the IBs within the gap are found to depend weakly on the dopant concentration and the relative distances of the dopant ions. In addition, for a more pertinent comparison to real materials, we present a practical way to combine and analyze the densities of states resulting from the energetically most probable microscopic structures. This multi-intermediate-band picture provides a platform to comprehend unexplained features of the recent experimental study on the material [X. Lv *et al.*, Solar Energy **103**, 480 (2014)].

DOI: 10.1103/PhysRevB.90.075154 PACS number(s): 71.55.Ak, 31.15.E−, 88.40.jn, 88.40.jp

I. INTRODUCTION

Third-generation photovoltaics have received a lot of attention due to the increasing demand for highly efficient sustainable energy production. Substantial advances have been made in the field of so-called intermediate-band (IB) solar cells [1]. The main theoretical basis for this idea was developed by Luque and Martí [2], motivated by a report on fabrication of a novel silicon solar cell [3], which had higher efficiency than the theoretical limit for *p-n* junction based solar cells [4]. Luque and Martí proved that introducing bands in the middle of the absorber's gap can ideally increase the efficiency of cells beyond the Shockley-Queisser limit. Later, they showed that under ideal conditions, the efficiency of IB solar cells can even exceed the efficiency of a tandem cell in which two cells are connected in series [5].

Recently, significant attention has been paid to creating an IB solar cell by manipulating copper-based chalcopyrites, which are one of the most used materials in industrial solar cells [6–11]. A set of studies suggests doping with transition metals as a possible solution, and preliminary electronic structure and thermodynamic calculations have been performed for such systems [6,7,9,12,13]. Some of those studies led to experimental fabrication of IB solar cells [10,11,14], which demonstrates the importance of computational modeling in this rapidly developing field. Very recently, Ti-doped $CuGaS_2$ (Ti-CGS, doping concentration $\sim 6.7 \times 10^{20}$ cm^{-3}) was synthesized through a solvothermal process, and a significant absorption increase was demonstrated [14].

This bloom in experimental advancements and findings [10,11,14–19] needs to be supported by theoretical efforts to foster faster and further improvements of IB solar cells. Accurate calculations serve this purpose the best and even help to refine some of the basic assumptions. In this work, we show that the conventional half-filled picture of the IBs is not necessarily the only way to understand, analyze, and engineer this class of materials. Using density functional theory (DFT) calculations with a hybrid exchange-correlation functional, we study the structures, energetics, band gap, and energy-level positions generated by doping Ti on Ga-substitutional sites in different geometries. We show that actually two sets of IBs are induced by Ti dopants, offering a better explanation for the experimental absorption spectra.

II. COMPUTATIONAL DETAILS

A true assessment of the optical properties of doped materials requires advanced methods that can predict the electronic structure, particularly the band gap, with an acceptable accuracy. Therefore, we use a hybrid exchange-correlation functional [20–25], HSE06, that has shown a significant improvement in accuracy with respect to many other functionals and methods, particularly for band-gap estimations. While even advanced many-body methods such as G_0W_0 or scCOHSEX fail to predict the band gap of CGS with acceptable accuracy [26], our calculations predict the value of 2.20 eV for the band gap, which is very close to the experimental range (2.4–2.53) [27–31] and shows that HSE06 suits our purpose well.

For the bulk calculations, we used a rectangular chalcopyrite supercell of 16 atoms (the structure $Cu_4Ga_4S_8$, space group 122:$I\bar{4}2d$). In a set of calculations with converged parameters [32–34], we relaxed the cell vectors to minimize the total energy and atomic positions until all forces on every individual atom are smaller than 0.01 eV/Å.

The relaxed cell parameters are $a = 5.361$ Å and $c = 10.539$ Å, which are in very good agreement with the experimental values [$a = 5.3512(6)$ Å, $c = 10.478(3)$ Å] [35]. We obtain the relaxed anion displacement parameter, u, to be 0.2557, which is within the experimental range of [0.25, 0.275] [36–38].

Next, we construct and optimize the doped structure. Experimental evidence [14], based on Raman spectroscopy, x-ray photoemission spectroscopy (XPS), and x-ray diffraction (XRD) characterization, shows that Ti atoms replace Ga at

substitutional sites and acquire the 3+ ionization state. We therefore performed a cell and ionic relaxation on the same supercell as above when one Ga atom is replaced by one Ti atom, and we calculated the cell parameters to be $a = 5.336$ Å, $c = 10.766$ Å. The cell volume increases due to the fact that the atomic radius of Ti^{3+} (0.76 Å) is larger than that of Ga^{3+} (0.62 Å). Moreover, the tetrahedral structure that Ti adopts with the four nearest-neighbor S atoms is not perfect after the relaxation, and two of the Ti-S bond lengths are slightly shorter than the other two (by less than 1%). This lowers the point group symmetry from T_d to C_{2v}.

In this article, we will mainly concentrate on the results for a 64-atom-supercell (duplicating the pristine cell in the $\hat{x}$ and $\hat{y}$ directions) where two Ga atoms are replaced by Ti so that we have $Cu_{16}Ga_{14}Ti_2S_{32}$ structure. Such a choice allows the study of various inherently existing random structures due to the growth process. The structure corresponds to a dopant concentration close to the experimental one ($\sim 1.7 \times 10^{21}$ cm^{-3}). Having two titanium atoms in the structure, we can study the effect of the random distribution of dopants on the electronic structure of the system. Furthermore, it enables spin alignment degrees of freedom of the system.

As we pointed out above, the volume relaxation for the smaller structure was not significant (1.2%). Therefore, in the 64-atom cases with one or two dopants, we keep the pristine cell parameters fixed ($a = 10.722$ Å, $c = 10.539$ Å), but the atomic positions are relaxed with a Perdew-Burke-Ernzerhof (PBE) functional. In the electronic structure calculations, however, we use HSE06 functionals.

III. RESULTS AND DISCUSSIONS

Considering the random substitution of two Ga atoms by Ti, there exists a set of possible combinations. We divide these combinations into four distinct classes of configurations based on the rough relative distance between the dopants (R), taking into account the periodic boundary condition. Let us assume that the first atom is replaced in the center of the cell. The possibilities for the second replacement are as follows: four atoms with $R = 3.81$ Å (2Ti-S), two with $R = 5.36$ Å (2Ti-M), eight with $R \simeq 6.5$ Å (2Ti-L), and one with $R \simeq 7.58$ Å (2Ti-XL) [39]. The last case posed numerical problems and will not be discussed.

We chose one structure from each class and performed spin-dependent calculations with two different constraints on the number of spin components. Namely, the difference between spin-up and spin-down components is forced to be either zero or two, and it is referred to as "spin-compensated" and "spin-polarized," respectively.

All results are tabulated in Table I. The spin-polarized 2Ti-L structure is energetically the most favorable structure, followed closely by 2Ti-M, where the spin-compensated and spin-polarized cases are basically degenerate (differing by 0.003 eV). Therefore, we can conclude that all three configurations could in principle exist at room temperature, although they have different weight factors. It is worth pointing out that we do not take spin-orbit coupling into account in these calculations, since we do not expect it to have a meaningful effect on our analysis.

TABLE I. The difference between the calculated total energies of different configuration classes. The class abundance or frequency in the calculated supercell (f), and the dopant relative distance for each class (R), are also shown.

Configurations	f	R	ΔE (eV)
2Ti-S	4	3.81 Å	
Polarized			0.335
Compensated			0.298
2Ti-M	2	5.36 Å	
Polarized			0.027
Compensated			0.024
2Ti-L	8	~6.5 Å	
Polarized			0.000
Compensated			0.204

A schematic comparison between the electronic structure of the pristine and the two different doped structures is given in Fig. 1. The states are aligned with respect to the lowest eigenenergy of the Ga 3d states. In all cases, the presence of Ti dopant atoms lowers the valence-band maximum (VBM), and pushes the conduction-band minimum (CBM) up, hence it widens the band gap to $\simeq$2.85 eV.

It is worth mentioning that the band gap increases with dopant concentration. We calculated the band gap for one and four Ti-substituted atoms in a 64-atom structure, to be $\simeq$2.3 and $\simeq$3.05 eV, respectively. Moreover, the element-specific projected density of states (PDOS) shows that the VBMs in both pristine and doped structures are mainly made of Cu and S orbitals, while the CBM is mostly made of Ga and S orbitals in pristine and mainly Ti orbitals in the doped structures [Fig. 2(a)].

More importantly, the Ti atoms induce two sets of intermediate bands in the lower and upper part of the band gap, where the lower one is filled and the upper one is empty. In each of these sets there are two spin bands, and in the

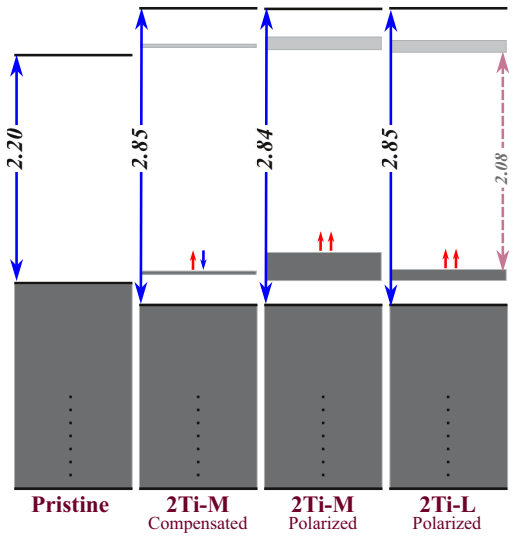

FIG. 1. (Color online) Schematic view of the energy-level positions for pristine and three differently doped structures.

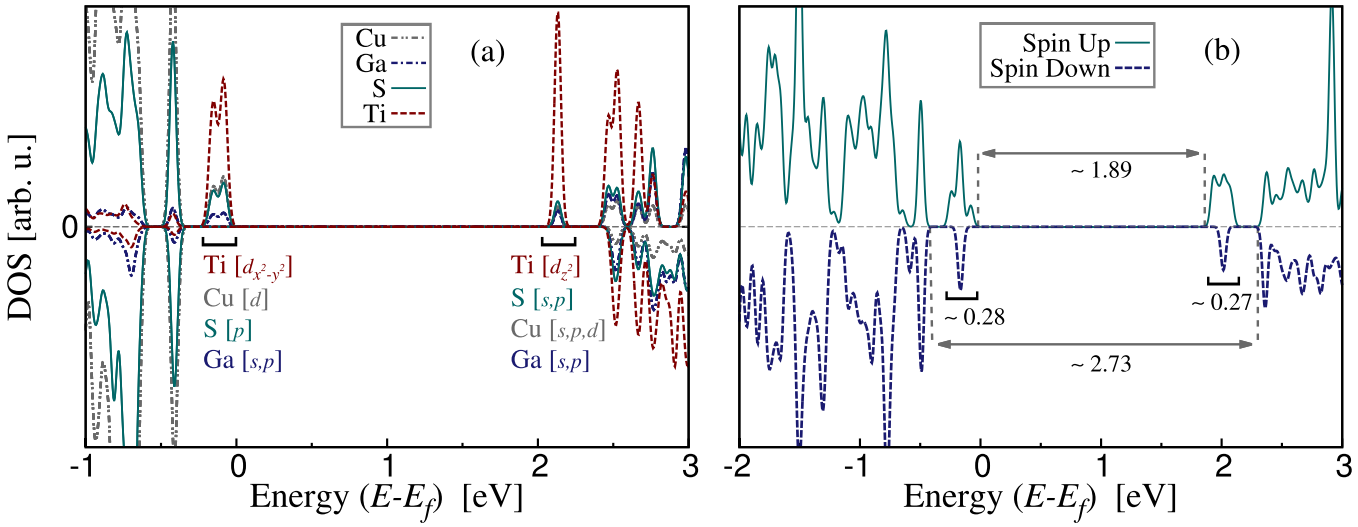

FIG. 2. (Color online) (a) The element-specific projected DOS for the 2Ti-L spin-polarized structure and (b) combined DOS made of the DOS of three different configurations, namely the 2Ti-M spin-polarized and spin-compensated configurations, as well as the 2Ti-L spin-polarized configuration, mixed with their corresponding weight factors. Note that an additional broadening of 0.05 eV has been applied.

spin-polarized configurations the upper and lower IBs are derived from the same spin component. We also verified that for other concentrations (one or four Ti dopant atoms in the 64-atom supercell), the IBs form roughly at similar distances from the VBM and the CBM, which suggests a fairly universal behavior exhibited by Ti as a dopant at Ga-substitutional sites.

Figure 2(a) illustrates the PDOS around the band gap of the 2Ti-L configuration, together with the share of each element in the IBs. The lower IBs consist mainly of titanium d orbitals ($\sim$60%) and the rest originates from the copper d orbitals ($\sim$20%) as well as sulfur p orbitals ($\sim$17%). Gallium s and p orbitals contribute less than 5% to the lower IBs. For the upper IBs, titanium d orbitals are building $\sim$75% of the DOS, while sulfur (s and p), copper (s, p, and d), and gallium (s and p) each contribute $\sim$8%.

The formation of IBs can be explained as follows. In the pristine material, the oxidation states of the elements are Cu^{+}, Ga^{3+}, and S^{2-}. Now if a Ga^{3+} ion is replaced by a Ti ion, it tends to have the same oxidation state and hence is in the Ti^{3+} state. Thus one $3d$ electron remains localized on the titanium ion and it forms a band in the middle of the gap. Lv *et al.* confirmed these oxidation states with the help of XPS experiments [14].

We also investigated the hybridization of the titanium $3d$ orbitals in the IBs. According to the crystal-field theory for the T_d point-group symmetry, the d_{z^2} and $d_{x^2-y^2}$ orbitals are energetically the lowest and degenerate. However, in the case of Ti atoms, the degeneracy is lifted: the $d_{x^2-y^2}$ orbitals mainly form the lower IBs, while the d_{z^2} orbitals construct the higher IBs, and their energy difference is $\sim$2 eV. Our PBE calculation found the splitting to be 0.2 eV, which shows the effect of using hybrid functionals in adjusting the split. However, such a large splitting by hybrid functionals is not unprecedented. For instance, Stroppa and Kresse [40] observed a very similar large splitting in Mn-doped GaN, and the results were supported by more accurate GW_0 calculations and experimental evidence.

Although the aforementioned point-group symmetry lowering, from T_d to C_{2v}, might induce a slight degeneracy lift (on the order of 100 meV), it cannot account for such a large energy difference. We thus interpret this splitting as an effect of different levels of hybridization and localization of the orbitals.

Figure 3 illustrates the spatial distribution of (a) the lower and (b) the upper IB states for the 2Ti-L spin-polarized case. From the figure, the $d_{x^2-y^2}$ and d_{z^2} shapes of Ti d orbitals are easily recognizable in the (a) and (b) parts, respectively (the z axis is normal to the plane of the figure).

Additionally, other valuable facts can be extracted from comparing the density of states. First, the electronic density of the upper IBs is much more localized on titanium sites than that of the lower IBs. Secondly, only those sulfur atoms that are immediately bonded to titanium atoms contribute to the IBs. However, all the copper atoms in the supercell have roughly an equal contribution to the electronic density of the lower IBs,

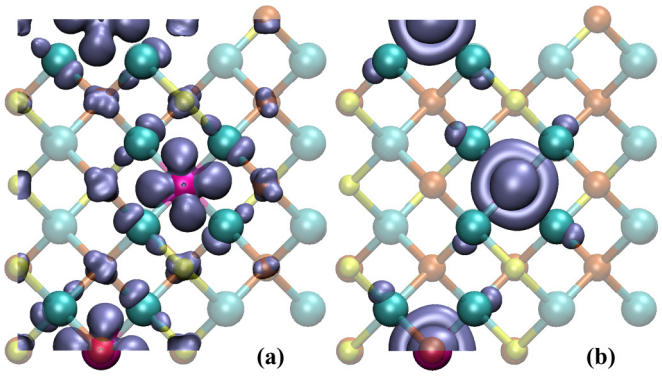

FIG. 3. (Color online) Cu ▶, Ga ▶, S ▶, Ti ▶. Spatial distribution of DOS for the (a) lower and (b) upper IBs of the 2Ti-L structure. Titanium atoms and their sulfur ligands are shown in bright colors while other atoms are shown in dull colors. The z axis is normal to the plane. Notice that Ga atoms carry no DOS in this particular isosurface, although it might seem so in the two-dimensional view.

while they do not play a significant role in the upper bands. This shows that the Ti-Ti interaction is largely mediated by copper electrons in the occupied states. Finally, we also see that the contribution of gallium atoms to IBs is negligible in both cases.

As mentioned earlier, three of the studied configurations can exist at room temperature since their energy difference is within thermal energies. As is shown in Fig. 1, the CBM and the VBM have the same energies for all these configurations, but the energy positions of IBs vary. In the following, we introduce a practical analysis, denoted combined DOS analysis, to better assess the actual density of states (band-gap width, IB width, etc.) that can be probed in the experiment. Considering our set of systems as forming a thermodynamic ensemble, the most probable microstates at room temperature, based on the formation energy, are both spin-polarized and compensated 2Ti-M, and the spin-polarized 2Ti-L. In addition, we assign the appropriate weight factor to the DOS of each microstate:

$$W_i = f_i \frac{e^{-\beta E_i}}{\sum_i f_i e^{-\beta E_i}}, \quad (1)$$

where f is the number of possible combinations in the class of structures which are (or in the 2Ti-L case, are assumed to be) geometrically equivalent, E is the formation energy of each microstate, and β should be calculated at the growth temperature. In this work, room temperature was used since in Ref. [14] the system was naturally annealed to room temperature. Here the weights are 0.31, 0.27, and 0.42 for the spin-polarized and compensated 2Ti-M, and spin-polarized 2Ti-L, respectively. The resulting DOS is shown in Fig. 2(b). It can be seen that both IB bands become approximately as wide as 0.3 eV, which is wider than IBs in any of the configurations [e.g., Fig. 2(a)]. Therefore, the IBs are both closer to each other and to the VBM and CBM. These distances might change somewhat depending on the concentration of dopants.

In light of our calculations, the experimental results of Lv *et al.* [14] can be understood and clarified fairly well. In Fig. 4(a) of their work, the experimental absorption spectrum is shown. There, the main peak of the absorption spectrum of $CuGaS_2$ appeared at around 2.5 eV and it was attributed to the band gap of the system, while in the doped system this peak was shifted to higher energy. The shift confirms that, as we showed in the calculations, the presence of titanium increases the band gap of the doped structure. The amount of this increase ($\sim$0.4 eV) is in good agreement with the calculated increase from 2.20 eV to $\sim$2.73 eV [see Fig. 2(b)].

In addition, in the experimental results of Lv *et al.* [14], three absorption edges are identified. The authors concluded that due to the IB, there are two additional sub-band-gap responses at 0.92 and 1.75 eV. However, the absorbance is relatively high also well below 0.92 eV, and some weak absorption edges could be present in the range of 0.6–0.9 eV. We believe that these could signal other absorption processes, and they may be related to the two sets of IBs in the band gap that we report. The low-energy absorbance can be explained by the fact that the two IB sets in the band gap are close to the VBM and CBM.

Finally, it should be noted that to fully explain the experimental observations, further systematic calculations are needed. For example, the excitonic effects and relaxation after the system absorbs a photon should be taken into account. The current calculations, nevertheless, provide the starting point to refine our understanding of the working principles of this class of materials.

IV. CONCLUSIONS

With a state-of-the-art hybrid functional calculation, we showed that Ti-substitutional doping of $CuGaS_2$ universally increases the band gap and induces two sets of intermediate bands. The multi-intermediate-band picture reported here is consistent with the recent experimental findings. We also examined the different possible substitutional configurations and found a systematically similar behavior. We therefore conclude that the conventional single (half-filled) IB picture should be extended to include a multiple (filled and empty) IB scenario.

These results and the gained insight widen our understanding and influence the efforts to engineer better and more efficient IB solar cells. They also call for further theoretical study on the efficiency of IB materials, including the new extended picture. Moreover, we suggest element-specific x-ray spectroscopy studies on this particular compound to probe the nature of the crucial d states of Ti and their interaction with the host material.

ACKNOWLEDGMENTS

This work was supported by the Academy of Finland (Contracts No. 1260204, No. 1259599, No. 1259526, and No. 1256211). We are grateful to CSC, IT Center for Science, for their generous computational time. We also thank Martti Puska, Laura Oikkonen, Peter Agoston, and Silvana Botti for fruitful discussion throughout the work.

[1] A. Luque, A. Martí, and C. Stanley, Nat. Photon. **6**, 146 (2012).
[2] A. Luque and A. Martí, Phys. Rev. Lett. **78**, 5014 (1997).
[3] J. Li, M. Chong, J. Zhu, Y. Li, J. Xu, P. Wang, Z. Shang, Z. Yang, R. Zhu, and X. Cao, Appl. Phys. Lett. **60**, 2240 (1992).
[4] W. Shockley and H. J. Queisser, J. Appl. Phys. **32**, 510 (1961).
[5] A. Luque and A. Mart, Progr. Photovoltaics: Res. Appl. **9**, 73 (2001).
[6] P. Palacios, K. Snchez, J. C. Conesa, and P. Wahnón, Phys. Status Solidi A **203**, 1395 (2006).
[7] P. Palacios, K. Snchez, J. Conesa, J. Fernndez, and P. Wahnón, Thin Solid Films **515**, 6280 (2007).
[8] I. Aguilera, P. Palacios, and P. Wahnón, Solar Energy Mater. Solar Cells **94**, 1903 (2010).
[9] P. Palacios, I. Aguilera, and P. Wahnón, Thin Solid Films **516**, 7070 (2008).

[10] B. Marsen, S. Klemz, T. Unold, and H.-W. Schock, Progr. Photovoltaics: Res. Appl. **20**, 625 (2012).
[11] P. Chen, M. Qin, H. Chen, C. Yang, Y. Wang, and F. Huang, Phys. Status Solidi A **210**, 1098 (2013).
[12] P. Palacios, I. Aguilera, P. Wahnn, and J. C. Conesa, J. Phys. Chem. C **112**, 9525 (2008).
[13] Y. Seminvski, P. Palacios, and P. Wahnn, Thin Solid Films **519**, 7517 (2011).
[14] X. Lv, S. Yang, M. Li, H. Li, J. Yi, M. Wang, G. Niu, and J. Zhong, Solar Energy **103**, 480 (2014).
[15] A. Luque, A. Marti, C. Stanley, N. Lopez, L. Cuadra, D. Zhou, J. L. Pearson, and A. McKee, J. Appl. Phys. **96**, 903 (2004).
[16] V. Popescu, G. Bester, M. C. Hanna, A. G. Norman, and A. Zunger, Phys. Rev. B **78**, 205321 (2008).
[17] S. Tomi, A. Mart, E. Antoln, and A. Luque, Appl. Phys. Lett. **99**, 053504 (2011).
[18] S. Dhomkar, U. Manna, L. Peng, R. Moug, I. Noyan, M. Tamargo, and I. Kuskovsky, Solar Energy Mater. Solar Cells **117**, 604 (2013).
[19] N. López, L. A. Reichertz, K. M. Yu, K. Campman, and W. Walukiewicz, Phys. Rev. Lett. **106**, 028701 (2011).
[20] We performed all calculations with the plane-wave code VASP, using the projector-augmented wave (PAW) method.
[21] G. Kresse and J. Hafner, Phys. Rev. B **47**, 558 (1993).
[22] G. Kresse and J. Furthmüller, Phys. Rev. B **54**, 11169 (1996).
[23] A. D. Becke, J. Chem. Phys. **98**, 1372 (1993).
[24] J. Heyd, G. E. Scuseria, and M. Ernzerhof, J. Chem. Phys. **118**, 8207 (2003).
[25] J. Heyd, G. E. Scuseria, and M. Ernzerhof, J. Chem. Phys. **124**, 219906 (2006).
[26] I. Aguilera, J. Vidal, P. Wahnón, L. Reining, and S. Botti, Phys. Rev. B **84**, 085145 (2011).
[27] J. L. Shay, B. Tell, H. M. Kasper, and L. M. Schiavone, Phys. Rev. B **5**, 5003 (1972).
[28] B. Tell, J. L. Shay, and H. M. Kasper, Phys. Rev. B **4**, 2463 (1971).
[29] C. Bellabarba, J. González, and C. Rincón, Phys. Rev. B **53**, 7792 (1996).
[30] N. Syrbu, I. Tiginyanu, L. Nemerenco, V. Ursaki, V. Tezlevan, and V. Zalamai, J. Phys. Chem. Solids **66**, 1974 (2005).
[31] J. Botha, M. Branch, P. Berndt, A. Leitch, and J. Weber, Thin Solid Films **515**, 6246 (2007).
[32] For the 16-atom and 64-atom systems, $4 \times 4 \times 2$ and $2 \times 2 \times 2$ sets of Monkhorst-Pack **k** points were chosen, respectively. We use the well-converged energy cutoff of 400 eV in these calculations.
[33] L. E. Oikkonen, M. G. Ganchenkova, A. P. Seitsonen, and R. M. Nieminen, J. Phys.: Condens. Matter **23**, 422202 (2011).
[34] L. E. Oikkonen, M. G. Ganchenkova, A. P. Seitsonen, and R. M. Nieminen, Phys. Rev. B **86**, 165115 (2012).
[35] A. H. Romero, M. Cardona, R. K. Kremer, R. Lauck, G. Siegle, C. Hoch, A. Muñoz, and A. Schindler, Phys. Rev. B **83**, 195208 (2011).
[36] J. Schneider, A. Ruber, and G. Brandt, J. Phys. Chem. Solids **34**, 443 (1973).
[37] S. C. Abrahams and J. L. Bernstein, J. Chem. Phys. **59**, 5415 (1973).
[38] H. W. Spiess, U. Haeberlen, G. Brandt, A. Ruber, and J. Schneider, Phys. Status Solidi B **62**, 183 (1974).
[39] The different configurations in each class are symmetrically equivalent, with the exception of the 2Ti-L class, in which there are two highly similar groups with the relative distance of 6.49 and 6.54 Å. We assume these two cases have sufficiently similar electronic structure so that only one of them is considered.
[40] A. Stroppa and G. Kresse, Phys. Rev. B **79**, 201201 (2009).